Statistical investigation of the frequency dependence of the chorus source mechanism of plasmaspheric hiss

Nigel P. Meredith, ¹ Jacob Bortnik, ² Richard B. Horne, ¹ Wen Li, ³ and Xiao-Chen Shen ³

Richard B. Horne, Nigel P. Meredith, British Antarctic Survey, Natural Environment Research Council, Madingley Road, Cambridge, CB3 0ET, England. (r.horne@bas.ac.uk; nmer@bas.ac.uk)

Jacob Bortnik, Department of Atmospheric and Oceanic Sciences, University of California, Los Angeles, 405 Hilgard Avenue, Los Angeles, CA 90095-1565, USA. (jbortnik@gmail.com)

Wen Li, Xiao-Chen Shen, Centre for Space Physics, Boston University, Boston, MA, USA. (wenli77@bu.edu; sdusxc@gmail.com)

¹British Antarctic Survey, Natural

Environment Research Council, Cambridge,

England

²Department of Atmospheric and Oceanic

Sciences, University of California, Los

Angeles, USA

³Centre for Space Physics, Boston

University, Boston, MA, USA

- 3 Abstract. We use data from eight satellites to statistically examine the
- 4 role of chorus as a potential source of plasmaspheric hiss. We find that the
- strong equatorial ($|\lambda_m| < 6^o$) chorus wave power in the frequency range 50
- $_{6}~< f < 200~\mathrm{Hz}$ does not extend to high latitudes in any MLT sector and is
- unlikely to be the source of the low frequency plasmaspheric hiss in this fre-
- ⁸ quency range. In contrast, strong equatorial chorus wave power in the medium
- $_{9}$ frequency range 200 < f < 2000 Hz is observed to extend to high latitudes
- and low altitudes in the pre-noon sector, consistent with ray tracing mod-
- elling from a chorus source and supporting the chorus to hiss generation mech-
- anism. At higher frequencies, chorus may contribute to the weak plasmas-
- $_{\mbox{\tiny 13}}$ pheric hiss seen on the dayside in the frequency range 2000 $< f < 3000~{\rm Hz}$
- band, but is not responsible for the weak plasmaspheric hiss on the night-
- side in the frequency range 3000 < f < 4000 Hz.

1. Introduction

Plasmaspheric hiss is a broadband, electromagnetic emission, that occurs below the electron gyrofrequency in the frequency range from ~20 Hz to several kHz (Li et al., 2015a). The waves, as their name implies, tend to be confined to the higher density regions associated with the Earth's plasmasphere (e.g., Thorne et al., 1973) and plasmaspheric plumes (e.g., Summers et al., 2008; Shi et al., 2019), where they tend to be strongest on the dayside during geomagnetically active conditions (Li et al., 2015a; Meredith et al., 2004; 2018).

Plasmaspheric hiss is an important magnetospheric emission due to its role in radiation
belt dynamics. It is largely responsible for the formation of the slot region between the
inner and outer radiation belt (Lyons and Thorne, 1973). Further out it contributes to
electron loss during geomagnetic storms (Lam et al., 2007) and the quiet time decay of
outer radiation belt electrons (Meredith et al., 2006a). It can also explain the slow decay
of the unusual narrow ring of multi-MeV electrons produced during the September 2012
geomagnetic storm (Thorne et al., 2013)

Despite over 45 years of research the origin of plasmaspheric hiss remains a topic of active debate. Ray tracing models show that chorus waves can propagate into the plasmasphere and evolve into plasmaspheric hiss (Bortnik et al., 2008, 2011a, 2011b; Chen et al., 2012a, 2012b; 2012c). This mechanism is also supported by observations which confirm some of the key predictions of this theory (Agapitov et al., 2018; Bortnik et al., 2009b; Li et al., 2015b, Meredith et al., 2013; Tsurutani et al., 2012; Wang et al., 2011). However, a recent study has suggested that it is unlikely that chorus directly contributes to a

significant fraction of hiss wave power (Hartley et al., 2019). Indeed, there is evidence to suggest that plasmaspheric hiss at low and medium frequencies (20 < f < 2000 Hz) can be generated by local amplification of the background whistler mode noise due to substorm injected electrons (Chen et al., 2014; Li et al., 2013; Su et al., 2018; Liu et al., 2019) and, at high frequencies (f > 2000 Hz), lightning-generated whistlers also play a role (Meredith et al., 2006b). Furthermore, He et al., (2019; 2020) have recently reported a new form of high frequency plasmaspheric hiss which they observe to peak on the dawn-side during active conditions and which they also attribute to local generation by substorm injected electrons.

To improve our understanding of the origin of plasmaspheric hiss and, in particular, to
examine the role of chorus as a potential source, we extended the ELF/VLF wave database
that we originally used to investigate evidence for chorus as the source of plasmaspheric
hiss (Meredith et al., 2013) by including ~ 3 years of data from the Van Allen Probes,
Radiation Belt Storm Probes (RBSP)-A and RBSP-B and an additional ~6 years of data
from each of the Time History of Events and Macroscale Interactions during Substorms
(THEMIS)-A, THEMIS-D and THEMIS-E. The satellites, associated instrumentation,
and data analysis techniques used to develop the model are briefly described in Section
The global morphology of the average intensities of plasmaspheric hiss as a function
of spatial location and frequency are presented and interpreted in Section 3. Finally our
results are discussed and our conclusions presented in Sections 4 and 5 respectively.

2. Instrumentation and Data Analysis

To construct a comprehensive database of plasmaspheric hiss and potentially-associated chorus in the inner magnetosphere we combined data from eight satellites. We used 2.8

years of data from Dynamics Explorer 1, 1 year of data from Double Star TC1, 10 years of data from Cluster 1, 7.8 years of data from THEMIS-A, THEMIS-D and THEMIS-E and 2.8 years of data from RBSP-A and RBSP-B. Details of the methods used to analyze the wave data from DE1, Double Star TC1, Cluster 1 and the THEMIS probes are given in Meredith et al. (2012) and those used to analyze the wave data from the Van Allen Probes are given in Li et al. (2015a).

Magnetosonic waves can potentially contaminate the emissions when the frequency becomes less than the lower hybrid resonance frequency. For the Van Allen Probe measurements we excluded magnetosonic waves, which typically have large wave normal angles
and hence low ellipticity values, by excluding waves with ellipticity less than 0.7. We
do not routinely have information on the wave ellipticity from the other satellites and a
different approach is required. Observations show that magnetosonic waves are tightly
confined to the equatorial region (e.g., Nemec et al., 2005) and we remove these waves to
first order by excluding emissions below the lower hybrid resonance frequency within $\pm 3^{\circ}$ of the geomagnetic equator.

We binned the wave power from each satellite in eight frequency bands between 10 Hz and 4000 Hz as a function of L^* , magnetic local time (MLT), magnetic latitude (λ_m) and geomagnetic activity as monitored by the AE index as detailed in Table 2 in Meredith et al., (2012). For the database L^* and MLT were computed using the Olson-Pfitzer quiet time model (Olson & Pfitzer, 1977) and the IGRF field at the middle of the appropriate year. Since the software is designed for particles and we are using it for waves we assume a local pitch angle of 90° in the calculation of L^* . We then combined the data from each of the satellites, weighting the data from each individual satellite by the corresponding

number of samples, to produce a combined wave database as a function of frequency band, L^* , MLT, λ_m and geomagnetic activity.

Addition of the new wave data allows us to extend the frequency coverage below 100 Hz enabling us to probe the origins of low frequency plasmaspheric hiss. Furthermore, at higher frequencies, both the statistics and coverage are significantly improved in the near-equatorial region. For example, the average number of samples of the plasma waves in the frequency range 200 < f < 500 Hz per L^* , MLT bin in the region $|\lambda_m| < 15^{\circ}$ for $2 < L^* < 8$ during active conditions, AE > 100 nT, with and without the new wave data is 23,776 and 661 respectively, increasing the average number of samples in each L^* , MLT bin by a factor of greater than 35. The extended database enables us to examine the global distribution of the wave power in the near-equatorial region at a latitudinal resolution of 6° , compared with 10° in Li et al. (2011) and 15° in Meredith et al. (2012; 2013), revealing new features.

3. Global Morphology

Chorus waves are typically generated close to the geomagnetic equatorial plane (LeDocq et al., 1998; Santolik and Gurnett 2003) by anisotropic distributions of electrons with energies in the range of approximately keV to ~100 keV (Li et al., 2010; Omura et al., 2008) injected into the inner magnetosphere during storms and substorms. If these chorus emissions are the source of plasmaspheric hiss then we would expect to see clear evidence of chorus extending from its generation region near the geomagnetic equator to higher latitudes and low altitudes where, according to theory, it can enter the plasmasphere and evolve into plasmaspheric hiss (Bortnik et al., 2008). For the purposes of this investigation we define low, medium and high frequency plasmaspheric hiss as having frequencies in

the ranges 20 < f < 200 Hz, 200 < f < 2000 Hz and 2000 < f < 4000 Hz respectively.

We then look for signatures of the chorus to hiss generation mechanism by examining the global distribution of the waves during active conditions, AE > 100 nT, as a function of frequency.

To examine the global distribution of the waves we plot the average wave intensity 108 during active conditions, when the waves tend to be enhanced, as a function of frequency 109 band, λ_m , L^* and MLT in Figures 1 and 2. To examine the dependence on latitude in 110 more detail, we also plot the global distribution of the waves in the meridional plane as 111 a function of frequency band and MLT sector in Figures 3 and 4. The four frequency 112 bands in the range 20-500 Hz are presented in Figures 1 and 3 and the four frequency 113 bands in the range 500-4000 Hz are presented in Figure 2 and 4. In the figures the results 114 are displayed for, from bottom to top, increasing frequency and, from left to right, either 115 increasing magnetic latitude (Figures 1 and 2) or increasing magnetic local time (Figures 3 and 4). The average intensities are shown in the large panels and the corresponding 117 sampling distributions in the small panels. In the meridional plots, Figures 3 and 4, dipole field lines and lines of constant magnetic latitude are included to help visualise the behaviour of the wave intensities as a function of L^* and $|\lambda_m|$. We also include the 120 wave data beyond $|\lambda_m| = 18^{\circ}$, but note that the coverage is much reduced at the higher 121 latitudes. 122

Two populations of waves can generally be seen in the equatorial region, $|\lambda_m| < 6^o$, (e.g., Figure 1a). An inner population which peaks on the dayside inside $L^* = \sim 5$, consistent with previous observations of plasmaspheric hiss (Li et al., 2015a; Meredith et al., 2004;

²⁶ 2018) and an outer population that peaks further out on the dawnside consistent with previous observations of whistler mode chorus (Li et al., 2011; Meredith et al., 2001; 2020).

3.1. Low Frequency Plasmaspheric Hiss

Strong equatorial ($|\lambda_m| < 6^o$) low frequency plasmaspheric hiss in the 100-200 Hz band 128 is observed on the dayside in the region $2.0 < L^* < 5.0$ (Figure 1d). Here, and elsewhere, we define regions of strong wave power as those with average wave intensities greater than 200 pT². These regions are color-coded red in the plots. Further out strong equatorial 131 chorus is observed primarily in the region $6.5 < L^* < 10$ from 22:00 to 08:00 MLT. Moving to higher latitudes, the hiss intensities weaken and the chorus intensities fall off 133 dramatically such that, in the region $12 < |\lambda_m| < 18^{\circ}$, there is no significant chorus power on the nightside and much reduced power in the region 06:00 to 08:00 MLT (Figure 1f). 135 Moving to even higher latitudes, there is no evidence for strong chorus wave power inside 136 $L^* = 9$ in any MLT sector (Figures 3e, 3f, 3g and 3h). Although not so strong, the 137 observed wave power follows a similar pattern of behaviour in the 50-100 Hz band. Here, 138 in the equatorial region, low frequency plasmaspheric hiss is observed primarily on the 139 dayside and weakens with increasing latitude (Figures 1g, 1h, 1i). Further out, chorus is 140 strongest in the equatorial region at $L^* > 7$ from 23:00 to 07:00 MLT (Figure 1g) and falls 141 off dramatically with increasing latitude (Figure 1h and 1i). Low frequency plasmaspheric 142 hiss is much weaker in the 20-50 Hz band (Figure 1j). However, we are unable to examine 143 chorus at higher L^* since the coverage is limited to $L^* < \sim 6$ due to the exclusion of 144 the THEMIS data, which suffers from variable background noise contamination in this frequency range. These results suggest that chorus is unlikely to be significant source of 146 low frequency plasmaspheric hiss (50 < f < 200 Hz) since strong chorus is not observed to

extend to high latitudes in any MLT sector. The source of the low frequency plasmaspheric
hiss in this frequency range is more likely to be local amplification of the background
whistler mode noise due to substorm-injected electrons in the outer plasmasphere (e.g.,
Chen et al., 2014; Li et al., 2013).

3.2. Medium Frequency Plasmaspheric Hiss

Strong equatorial medium frequency plasmaspheric hiss in the 200-500 Hz band is observed in the equatorial region on the dayside from $1.5 < L^* < 5.0$ (Figure 1a). The region 153 of strong waves also extends for a few hours into the pre-dawn and post dusk sectors, albeit for smaller ranges of L^* . Further out, strong equatorial chorus is observed from 21:00 155 MLT through dawn to 13:00 MLT primarily in the region $5 < L^* < 10$, with the inner boundary of the strong chorus moving progressively to larger values of L^* with decreasing 157 and increasing MLT in the pre-midnight and pre-noon sectors respectively (Figure 1a). 158 Moving to higher latitudes the plasmaspheric hiss remains strong (Figures 1b and 1c). The 159 chorus intensities also remain strong in the pre-noon sector where they are also observed 160 to extend to lower L^* (Figures 1b and 1c). In fact, strong waves are observed all the way 161 from the equator to very high latitudes in the region $5 < L^* < 7$ in the pre noon sector 162 (Figure 3b). Indeed, a second intensity peak is seen at high latitudes and low altitudes 163 due to the convergence of the magnetic field lines. On the nightside the strong chorus is 164 tightly confined to the equatorial region, being largely restricted to the regions $|\lambda_m| < 6^{\circ}$ 165 and $|\lambda_m| < 12^o$ in the pre-midnight and post-midnight sectors respectively (Figures 3d 166 and 3a). 167

We observe a similar pattern of behaviour for medium frequency plasmaspheric hiss in the 500-1000 Hz band, although the overall extent of the regions of strong plasmaspheric

hiss and chorus are reduced (Figure 2j). For example, in this frequency range the strong equatorial plasmaspheric hiss is observed primarily on the dayside in the region 2 < 171 $L^* < 4$. Strong equatorial chorus is observed from 21:00 MLT through dawn to noon 172 but the spatial extent is restricted to the range $5 < L^* < 8$. Unlike the situation at 173 lower frequencies strong waves are absent in the region $8 < L^* < 10$. Moving to higher 174 latitudes plasmaspheric hiss remains strong on the dayside (Figures 2k and 2l). The 175 chorus intensities remain strong in the pre-noon sector (Figures 2k and 2l) and intensify 176 post-noon from 12:00 to 14:00 MLT in the range $5 < L^* < 7$ (Figure 21). The chorus also 177 remains strong in a restricted zone in the pre-dawn sector from 02:00 to 06:00 MLT in 178 the region $5 < L^* < 6$ for $12 < \lambda_m < 18^{\circ}$. Moving further from the equator, strong waves 179 are observed to extend to high latitudes and low altitudes in the region $5 < L^* < 7$ in the 180 pre noon sector (Figure 4n). 181

Medium frequency plasmaspheric hiss is weaker in the 1000-2000 Hz band, with intensities of the order of 100 pT² on the dayside (Figure 2g). Strong equatorial chorus is still observed further out, although it is more tightly confined, being observed from 21:00 MLT through dawn to 10:00 MLT, typically from $4.5 < L^* < 6$. Moving away from the equator the strong chorus is mostly confined to the region 03:00 to 14:00 MLT for $12 < \lambda_m < 18^o$ (Figure 2i). Chorus remains strong in the region $4.5 < L^* < 6$ to high latitudes and low altitudes, but only in the pre-noon sector (Figure 4j).

Our statistical observations demonstrate that strong chorus waves in the frequency range 200 < f < 2000 Hz are present all the way from the equatorial region to high latitudes and low altitudes in the pre-noon sector, consistent with ray tracing studies from an equatorial chorus source region (Bortnik et al., 2007). The intensity of plasmaspheric hiss

is weaker in the 1000-2000 Hz band despite strong chorus being present further out and 193 this is consistent with ray tracing theory which suggests that waves have more difficulty 194 accessing the plasmasphere at higher frequencies (Bortnik et al., 2007). We note that 195 strong hiss is observed in the afternoon sector with no immediate counterpart in chorus 196 activity in the same meridional plane at higher L^* . However, off-meridional propagation 197 can be very effective in the afternoon sector during geomagnetic storms due to strong 198 azimuthal plasma density gradients enabling rays to propagate eastwards where they can 199 potentially explain the strong plasmaspheic hiss emissions in the post-noon sector during 200 active times (Chen et al., 2009). 201

3.3. High Frequency Plasmaspheric Hiss

High frequency plasmaspheric hiss is much weaker than both low and medium frequency 202 plasmaspheric hiss, and becomes weaker with increasing frequency. In the 2000-3000 Hz 203 band intensities of the order 10 pT² are observed on the dayside in the region $2.0 < L^* <$ 204 4.0 (Figure 2d). Further out, strong equatorial chorus intensities is observed from 23:00 205 to 09:00 MLT, typically from $4.0 < L^* < 5.5$. Moving away from the equator the strong 206 chorus is mostly confined to the region 03:00 to 12:00 MLT for $12 < \lambda_m < 18^{\circ}$ (Figure 2f). 207 The strong chorus wave power does not extend to higher latitudes although weaker levels 208 of chorus power extend to low altitudes in the region $4 < L^* < 5$ on the dayside (Figures 209 4f and 4g). At higher frequencies, 3000-4000 Hz, the high frequency plasmaspheric hiss 210 wave power is even weaker, with largest intensities less than a few pT^2 on the dayside. 211 Here the intensities peak on the nightside rather than the dayside suggesting a different 212 source. Strong equatorial chorus is observed from 23:00 to 09:00 MLT, typically from 4.0 213 $< L^* < 5.0$ (Figure 2a) with the region of strong wave power moving progressively to larger MLT with increasing latitude (Figures 2c and 2d). Weak power extends to high latitudes in the pre-noon sector in the region $4 < L^* < 5$ but it is not related to any significant levels of plasmaspheric hiss inside the plasmapause. These results suggest that chorus may contribute to the observed intensities in the 2000-3000 Hz band but not at higher frequencies where the distribution of the wave power is completely different. This weaker population of high frequency plasmaspheric hiss on the nightside is more likely to be produced by lightning generated whistlers (e.g., Meredith et al., 2006b).

4. Discussion

The new study reveals some interesting features in the global distribution of chorus in 222 the pre-dawn sector. Here the waves tend to extend to higher latitudes at lower L^* for 223 frequencies above 500 Hz. For example, at $L^* = 7$, 6 and 5 the strongest waves in the 224 500-1000 Hz band are confined to within 6, 12 and 18° respectively. Moving to higher 225 frequencies, for any given L^* the strong equatorial chorus, if present, tends to be more tightly confined to the equatorial plane. However, at lower frequencies the chorus tends to be mostly confined to within 9° of the geomagnetic equator. In contrast, in the pre-noon sector, the waves can extend to much higher latitudes. We suggest that the behaviour of the chorus wave power outside the generation region is dominated by Landau damping which is less efficient at higher frequencies and higher values of L^* and less efficient in the 231 pre-noon sector (Bortnik et al., 2007). 232 He et al., (2020) recently conducted a statistical survey of high frequency plasmaspheric 233

He et al., (2020) recently conducted a statistical survey of high frequency plasmaspheric hiss, first reported in He et al., (2019), and showed evidence for enhanced waves in the plasmasphere on the dawn-side during active conditions. Specifically, they showed evidence for enhanced wave power in the frequency band from 2000 Hz to $0.5f_{ce}$ which increased with

increasing geomagnetic activity and also moved to lower L^* with increasing geomagnetic 237 activity. We see no evidence for enhanced plasmaspheric hiss at high frequencies in the dawn sector. We do, however, see evidence of enhanced chorus in this region. While we do 239 not discriminate between the waves inside and outside of the plasmapause in this study, in previous work we demonstrated that the plasmapause is typically around L=4.5 in 241 the pre-dawn sector during active conditions (Meredith et al., 2004; 2008). Furthermore, 242 the general inward movement of the region of enhanced chorus emissions with increasing 243 frequency (Figure 1d, 1a, 2j, 2g, 2d, 2a) is consistent with its dependence on the electron 244 gyrofrequency which increases with decreasing L (see, e.g., Figure 3 in Meredith et al. 245 (2013)). Our observations suggest that the strong waves at frequencies in the 2000-4000 Hz bands in the region $4.0 < L^* < 5.5$ on the dawnside (Figures 2d and 2a) are chorus 247 waves outside the plasmapause. The results also suggest that the waves observed at f> 2000 Hz on the dawnside at L > 4.0 during active conditions by He et al., (2020) are predominantly chorus waves outside the plamsasphere. 250

Hartley et al. (2019) recently suggested that chorus waves rarely exist with the wave vector orientation required to enter the plasmasphere and that the waves that are observed with the orientation required to propagate into the plasmasphere do not carry a substantial fraction of the wave power, bringing into question the efficacy of the chorus to hiss mechanism. However, our statistical study reveals strong wave power at high latitudes and low altitudes in the frequency range 200 < f < 2000 Hz linked to strong equatorial chorus wave power. The results suggest that significant chorus power can propagate to these locations, from where, according to theory, the waves can enter the plasmasphere and evolve into plasmaspheric hiss (Bortnik et al., 2008). The reason for the disparity in

these contradictory conclusions could be related to the method used to calculate the wave normal angles in the Hartley et al. (2019) study. The wave normal angles are derived from 261 486 ms waveforms recorded every 6 seconds and do not capture the full chorus elements 262 or examine them in detail. To take into account the variability of the wave vector orien-263 tation Hartley et al. (2019) assumed a 20° wide distribution of wave normal angles and 264 azimuthal angles centered on the mean values. However, this technique does not capture 265 the full range of wave vector orientations that can be present in a chorus element. For 266 example, Santolik et al. (2014) conducted a systematic analysis of 2230 chorus subpackets 267 in the morning-side equatorial region at R \sim 5 Earth radii and showed that waves in the 268 frequency range $0.2f_{ce} < f < 0.4f_{ce}$ with large amplhttps://doi.org/10.5285/151a855f-269 d030-485b-a2dd-4ea874e59bf6itudes, of the order of hundreds of pT, can extend to wave 270 normal angles of 30° and above. More recently, Crabtree et al. (2017), using Bayesian spectral analysis, found that after the first chorus few sub-elements, the wave normal angle and azimuthal angle change continuously within each sub-element, extending to intermediate wave normal angles and covering the full range of azimuthal angles. To comprehensively examine the chorus to his mechanism using wave vector orientations in the near-equatorial plane a thorough analysis of the fine structure of the chorus wave normal 276 and azimuthal angles would be required.

5. Conclusions

We have used our extended database of ELF/VLF waves to statistically examine the role of chorus as the source of plasmaspheric hiss. Our principal conclusions are:

- 1). Strong equatorial chorus observed during active conditions in the frequency range 50 < f < 200 Hz is not observed to extend to high latitudes and is thus not likely to be the source of low frequency plasmaspheric hiss.
- 283 2). Strong equatorial chorus observed during active conditions in the frequency range 294 200 < f < 2000 Hz is observed to extend to higher latitudes and low altitudes, principally in the pre-noon sector, consistent with ray tracing modelling from a chorus source, 295 suggesting that chorus is an important source of medium frequency plasmaspheric hiss.
- 3). Chorus in the frequency range 2000 < f < 3000 Hz is observed to extend to higher latitudes albeit at much weaker levels, principally in the pre-noon sector during active times, where it may contribute to the weak plasmaspheric hiss seen on the dayside.
- 4). Chorus does not extend to high latitudes on the nightside in any frequency range and is unlikely to be the source of the very weak plasmaspheric hiss observed primarily on the nightside in the frequency range 3000 < f < 4000 Hz.

Data Availability Statement

The results and data shown in this paper can be downloaded from the U.K. Polar
Data Centre (https://data.bas.ac.uk and https://doi.org/10.5285/151a855f-d030-485ba2dd-4ea874e59bf6).

Acknowledgments.

293

297

We acknowledge the CDAWeb (https://cdaweb.sci.gsfc.nasa.gov/index.html/) for the
provision of the DE-1 wave data. We thank LPCEE laboratory (Orléans, France)
for their help in the analysis of this wave data. We thank the STAFF-DWP instrument team for provision of the Double Star TC1 data which is available at
the Cluster Science Archive (https://www.cosmos.esa.int/web/csa). We thank NASA

contract NAS5-02099 and V. Angelopoulos for use of data from THEMIS Mis-Specifically, we thank O. Le Contel and A. Roux for use of SCM data, sion. 304 which is available from http://themis.ssl.berkeley.edu/data/themis/. 305 ful for the Van Allen Probes data from the EMFISIS instrument obtained from 306 https://emfisis.physics.uiowa.edu/data/index. We acknowledge the NSSDC Omniweb for 307 the provision of the geomagnetic activity indices used in this report. The research leading 308 to these results has received funding from the Natural Environment Research Council 309 Highlight Topic grant NE/P01738X/1 (Rad-Sat) and the NERC grants NE/V00249X/1 310 (Sat-Risk) and NE/R016038/1. JB would like to acknowledge support from NASA grant 311 NNX14AI18G, and RBSP-ECT and EMFISIS funding provided by JHU/APL contracts 312 967399 and 921647 under NASA's prime contract NAS5-01072. WL and XS would like 313 to acknowledge support from NASA grants 80NSSC20K0698 and 80NSSC19K0845, NSF 314 grant AGS-1847818, and the Alfred P. Sloan Research Fellowship FG-2018-10936.

References

- Agapitov, O., Mourenas, D., Artemyev, A., Mozer, F. S., Bonnell, J. W., Angelopoulos, V., Shastun, V., & Krasnoselskikh, V. (2018). Spatial extent and temporal correlation of chorus and hiss: Statistical results from multipoint THEMIS observations. *Journal of Geophysical Research: Space Physics*, 123, 83178330. https://doi.org/10.1029/2018JA025725
- Bortnik, J., Thorne, R. M., & Meredith N. P. (2007). Modeling the propagation characteristics of chorus using CRRES suprathermal electron fluxes. *Journal of Geophysical*
- 323 Research, 112, A08204, doi:10.1029/2006JA012237

- Bortnik, J., Thorne, R. M. & Meredith N. P. (2008). The unexpected origin of plasmas-
- pheric hiss from discrete chorus emissions. *Nature*, 452, 62-66, doi:10.1038/nature06741
- Bortnik, J., Li, W., Thorne, R. M., Angelopoulos, V., Cully, C., Bonnell, J., Le Contel, O.,
- & Roux, A. (2009). An observation linking the origin of plasmaspheric hiss to discrete
- chorus emissions. Science, 324(5928), 775778. https://doi.org/10.1126/science.1171273
- Bortnik, J., L. Chen, W. Li, R. M. Thorne, & R. B. Horne (2011a). Modeling the evolution
- of chorus waves into plasmaspheric hiss, Journal of Geophysical Research, 116, A08221,
- doi:10.1029/2011JA016499
- Bortnik, J., L. Chen, W. Li, R. M. Thorne, N. P. Meredith, & R. B. Horne (2011b).
- Modeling the wave power distribution and characteristics of plasmaspheric hiss, *Journal*
- of Geophysical Research, 116, A12209, doi:10.1029/2011JA016862
- Chen, L., Bortnik, J., Li, W., Thorne, R. M., & Horne, R. B. (2012a). Modeling the
- properties of plasmaspheric hiss: 1. Dependence on chorus wave emission, Journal of
- 337 Geophysical Research, 117, A05201, doi:10.1029/2011JA017201
- Chen, L., Bortnik, J., Li, W., Thorne, R. M., & Horne, R. B. (2012b). Modeling the
- properties of plasmaspheric hiss: 2. Dependence on the plasma density distribution,
- ³⁴⁰ Journal of Geophysical Research, 117, A05202, doi:10.1029/2011JA017202
- Chen, L., Li, W., Bortnik, J., & Thorne, R. M. (2012c). Amplification of whistler-
- mode hiss inside the plasmasphere, Geophysical Research Letters, 39, L08111,
- doi:10.1029/2012GL051488
- ³⁴⁴ Chen, L., Thorne, R. M., Bortnik, J., Li, W., Horne, R. B., Reeves, G. D., et al. (2014).
- Generation of unusually low frequency plasmaspheric hiss. Geophysical Research Letters,
- ³⁴⁶ 41, 57025709. https://doi.org/10.1002/2014GL060628

- Crabtree, C., Tejero, E., Ganguli, G., Hospodarsky, G. B., & Kletzing, C. A. (2017).
- Bayesian spectral analysis of chorus subelements from the Van Allen Probes, Journal
- of Geophysical Research Space Physics, 122, 60886106, doi:10.1002/2016JA023547
- 350 Hartley, D. P., Kletzing, C. A., Chen, L., Horne, R. B., & Santol O. (2019).
- Van Allen Probes observations of chorus wave vector orientations: Implications
- for the chorus-to-hiss mechanism. Geophysical Research Letters, 46, 2337 2346.
- https://doi.org/10.1029/2019GL082111
- ³⁵⁴ He, Z., Chen, L., Liu, X., Zhu, H., Liu, S., Gao, Z., & Cao, Y. (2019). Local generation of
- high-frequency plasmaspheric hiss observed by Van Allen Probes. Geophysical Research
- Letters, 46, 11411148. https://doi.org/10.1029/2018GL081578
- ³⁵⁷ He, Z., Yu, J., Chen, L., Xia, Z., Wang, W., Li, K., & Cui, J. (2020). Statistical study on
- locally generated high-frequency plasmaspheric hiss and its effect on suprathermal elec-
- trons: Van Allen Probes observation and quasi-linear simulation. Journal of Geophysical
- Research: Space Physics, 125, e2020JA028526. https://doi.org/10.1029/2020JA028526
- Lam, M. M., Horne, R. B., Meredith, N. P., & Glauert, S. A. (2007). Modeling the effects
- of radial diffusion and plasmaspheric hiss on outer radiation belt electrons. *Geophysical*
- ³⁶³ Research Letters, 34, L20112. https://doi.org/10.1029/2007GL031598
- LeDocq, M. J., Gurnett, D. A., & Hospodarsky, G. B. (1998). Chorus source locations
- from VLF Poynting flux measurements with the Polar spacecraft. Geophysical Research
- Letters, 25, 40634066. https://doi.org/10.1029/1998GL900071, 1998
- Li, W., Thorne, R. M., Nishimura, Y., Bortnik, J., Angelopoulos, V., McFadden, J.
- P., et al. (2010). THEMIS analysis of observed equatorial electron distributions re-
- sponsible for the chorus excitation. Journal of Geophysical Research, 115, A00F11.

- https://doi.org/10.1029/2009JA014845
- Li, W., Bortnik, J., Thorne, R. M., & Angelopoulos, V. (2011). Global distribution of wave
- amplitudes and wave normal angles of chorus waves using THEMIS wave observations.
- Journal of Geophysical Research, 116, A12205. https://doi.org/10.1029/2011JA017035
- Li, W., et al. (2013). An unusual enhancement of low-frequency plasmaspheric hiss in the
- outer plasmasphere associated with substorm-injected electrons. Geophysical Research
- 376 Letters, 40, 37983803, doi:10.1002/grl.50787
- Li, W., Ma, Q., Thorne, R. M., Bortnik, J., Kletzing, C. A., Kurth, W. S., Hospodarsky,
- G. B., & Nishimura, Y. (2015a). Statistical properties of plasmaspheric hiss derived from
- Van Allen Probes data and their effects on radiation belt electron dynamics. Journal of
- 380 Geophysical Research Space Physics, 120, 3393-3405. doi: 10.1002/2015JA021048
- Li, W., Chen, L., Bortnik, J., Thorne, R. M., Angelopoulos, V., Kletzing, C. A., Kurth,
- W. S., & Hospodarsky, G. B. (2015b). First evidence for chorus at a large geocentric
- distance as a source of plasmaspheric hiss: Coordinated THEMIS and Van Allen Probes
- observation, Geophysical Research Letters, 42, 241248, doi:10.1002/2014GL062832
- 385 Liu, N., Su, Z., Gao, Z., Zheng, H., Wang, Y., Wang, S. et al. (2020).
- 386 Comprehensive observations of substorm-enhanced plasmaspheric hiss generation,
- propagation, and dissipation. Geophysical Research Letters, 47, e2019GL086040.
- https://doi.org/10.1029/2019GL086040
- Lyons, L. R., & Thorne, R. M. (1973). Equilibrium structure of radiation belt electrons.
- Journal of Geophysical Research, 78 (13), 2142-2149, doi:10.1029/JA078i013p02142
- Meredith, N. P., Horne, R. B., & Anderson, R. R. (2001). Substorm de-
- pendence of chorus amplitudes: Implications for the acceleration of electrons

- to relativistic energies. Journal of Geophysical Research, 106(A7), 13,16513,178.
- https://doi.org/10.1029/2000JA900156
- Meredith, N. P., Horne, R. B., Thorne, R. M., Summers, D., & Anderson, R. R. (2004).
- Substorm dependence of plasmaspheric hiss. Journal of Geophysical Research, 109,
- ³⁹⁷ A06209. https://doi.org/1029/2004JA010387
- Meredith, N. P., Horne, R. B., Glauert, S. A., Thorne, R. M., Summers, D., Albert,
- J. M., & Anderson, R. R. (2006a). Energetic outer zone electron loss timescales
- during low geomagnetic activity. Journal of Geophysical Research, 111, A05212
- https://doi.org/10.1029/2005JA011516
- Meredith, N. P., Horne, R. B., Clilverd, M. A., Horsfall, D., Thorne, R. M., & Anderson,
- R. R. (2006b) Origins of plasmaspheric hiss. Journal of Geophysical Research, 111,
- 404 A09217, doi:10.1029/2006JA011707
- Meredith, N. P., Horne, R. B., Sicard-Piet, A., Boscher, D., Yearby, K. H., Li,
- W., & Thorne, R. M. (2012). Global model of lower band and upper band chorus
- from multiple satellite observations. Journal of Geophysical Research, 117, A10225.
- https://doi.org/10.1029/2012JA017978
- Meredith, N. P., Horne, R. B., Bortnik, J., Thorne, R. M., Chen, L., Li, W., & Sicard-Piet,
- A. (2013). Global statistical evidence for chorus as the embryonic source of plasmas-
- pheric hiss. Geophysical Research Letters, 40, 2891-2896, doi:10.1002/grl.50593
- Meredith, N. P., Horne, R. B., Kersten, T., Li, W., Bortnik, J., Sicard, A., &
- Yearby, K. H. (2018). Global model of plasmaspheric hiss from multiple satel-
- lite observations. Journal of Geophysical Research: Space Physics, 123, 4526-4541.
- https://doi.org/10.1029/2018JA025226

- Meredith, N. P., Horne, R. B., Shen, X.-C., Li, W., & Bortnik, J. (2020). Global model of
- whistler mode chorus in the near-equatorial region ($|\lambda_m| < 18^{\circ}$). Geophysical Research
- Letters, 47. https://doi.org/10.1029/2020GL087311
- Němec, F., Santolík, O., Gereová, K., Macŭsová, E., Laakso, H., de Conchy, Y., Maksi-
- movic, M., & Cornilleau-Wehrlin, N. (2006). Equatorial noise: Statistical study of its
- localization and the derived number density. Advances in Space Research, 37, 610 616,
- doi: 10.1016/j.asr.2005.03.025
- Olson, W. P., & Pfitzer, K. (1977). Magnetospheric magnetic field modelling annual sci-
- entific report, AFOSR Contract No. F44620-75-c-0033
- Omura, Y., Katoh, Y., & Summers, D. (2008). Theory and simulation of the gen-
- eration of whistler-mode chorus. Journal of Geophysical Research, 113, A04223.
- https://doi.org/10.1029/2007JA012622
- Santolík, O., Gurnett, D. A., Pickett, J. S., Parrot, M., & Cornilleau-Wehrlin, N. (2003).
- Spatio-temporal structure of storm-time chorus. Journal of Geophysical Research, 108,
- 430 1278, doi:10.1029/2002JA009791
- Santolík, O., Kletzing, C. A., Kurth, W. S., Hospodarsky, G. B., & Bounds, S. R. (2014).
- Fine structure of large-amplitude chorus wave packets Geophysical Research Letters, 41,
- 293299, doi:10.1002/2013GL058889
- shi, R., Li, W., Ma, Q., Green, A., Kletzing, C. A., Kurth, W. S., et al. (2019). Properties
- of whistler mode waves in Earth's plasmasphere and plumes. Journal of Geophysical
- Research: Space Physics, 124, 10351051. https://doi.org/10.1029/2018JA026041
- Su, Z., Liu, N., Zheng, H., Wang, Y., & Wang, S. (2018). Multipoint observations of night-
- side plasmaspheric hiss generated by substorm-injected electrons. Geophysical Research

- Letters, 45, 10,92110,932. https://doi.org/10.1029/2018GL079927
- Summers, D., Ni, B., Meredith, N. P., Horne, R. B., Thorne, R. M., Mold-
- win, M. B., & Anderson, R. R. (2008). Electron scattering by whistler-mode
- ELF hiss in plasmaspheric plumes. Journal of Geophysical Research, 113, A04219,
- https://doi.org/10.1029/2007JA012678
- 444 Thorne, R. M., Smith, E. J., Burton, R. K., & Holzer, R. E. (1973).
- Plasmaspheric hiss. Journal of Geophysical Research, 78(10), 15811596.
- https://doi.org/10.1029/JA078i010p01581
- ⁴⁴⁷ Thorne, R. M., Li, W., Ni, B., Ma, Q., Bortnik, J., Baker, D. N., et al. (2013). Evolution
- and slow decay of an unusual narrow ring of relativistic electrons near L~3.2 follow-
- ing the September 2012 magnetic storm. Geophysical Research Letters, 40, 35073511.
- https://doi.org/10.1002/grl.50627
- Tsurutani, B. T., Falkowski, B. J., Verkhoglyadova, O. P., Pickett, J. S., Santol O.,
- & Lakhina, G. S. (2012). Dayside ELF electromagnetic wave survey: A Polar sta-
- tistical study of chorus and hiss, Journal of Geophysical Research, 117, A00L12,
- doi:10.1029/2011JA017180.
- 455 Wang, C., Zong, Q., Xiao, F., Su, Z., Wang, Y., & Yue, C. (2011). The rela-
- tions between magnetospheric chorus and hiss inside and outside the plasmasphere
- boundary layer: Cluster observation. Journal of Geophysical Research, 116, A07221,
- doi:10.1029/2010JA016240

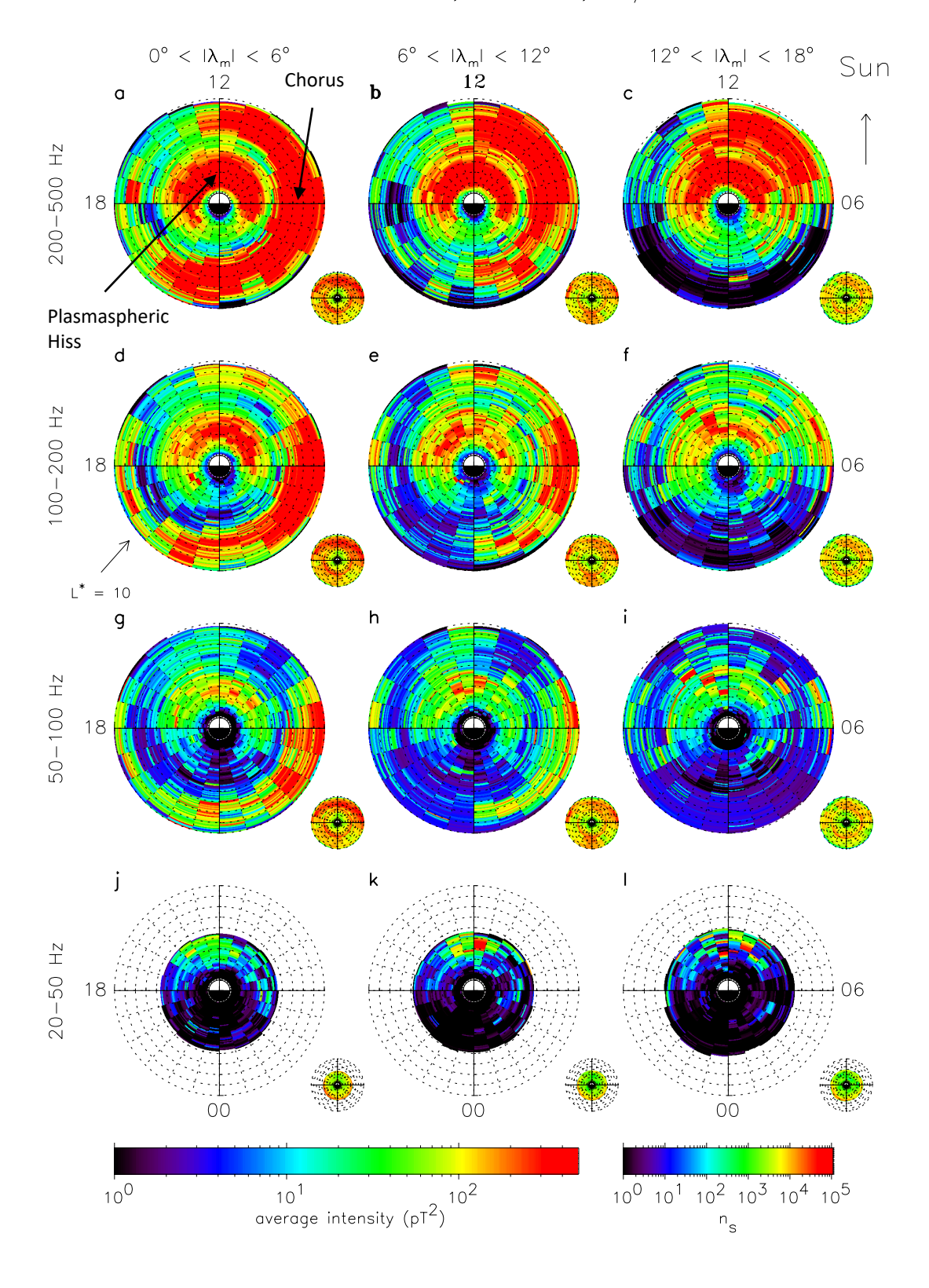
Figure 1. Global maps of the average wave intensity in the frequency range 20 < f < 500 Hz during active conditions (AE > 100 nT) as a function of L^* and MLT for, from bottom to top, increasing frequency band and, from left to right, increasing magnetic latitude. The maps extend linearly out to $L^* = 10$ with noon at the top and dawn to the right. The average intensities are shown in the large panels and the corresponding sampling distributions in the small panels.

Figure 2. Global maps of the average wave intensity in the frequency range 500 < f < 4000 Hz during active conditions (AE > 100 nT) as a function of L^* and MLT for, from bottom to top, increasing frequency band and, from left to right, increasing magnetic latitude. The maps extend linearly out to $L^* = 10$ with noon at the top and dawn to the right. The average intensities are shown in the large panels and the corresponding sampling distributions in the small panels.

Figure 3. Global maps of the average wave intensity in the frequency range 20 < f < 500 Hz during active conditions (AE > 100 nT) in the meridional plane for, from bottom to top, increasing frequency and, from left to right, increasing MLT. The average intensities are shown in the large panels and the corresponding sampling distributions in the small panels

Figure 4. Global maps of the average wave intensity in the frequency range 500 < f < 4000 Hz during active conditions (AE > 100 nT) in the meridional plane for, from bottom to top, increasing frequency and, from left to right, increasing MLT. The average intensities are shown in the large panels and the corresponding sampling distributions in the small panels

Whistler Mode Waves, 20-500 Hz, AE \rangle 100 nT



Whistler Mode Waves, 500-4000 Hz, AE \rangle 100 nT

